Time constraints on hydrocarbon migration and caprock formation recorded by calcite spar in a Carboniferous-Permian carbonate-evaporite succession, Finnmark Platform, Barents Sea

Malcolm S.W. Hodgskiss[1], Nivedita Thiagarajan[2], Yue Wang[1], Niels Rameil[3], Harald Brunstad[3], Erik Hammer[3], Jon Halvard Pedersen[3], Kalle Kirsimae[4], Atle Mørk, Aivo Lepland[1, 4]

[1]*Geological Survey of Norway, Trondheim 7040, Norway*
[2]*Division of Geological and Planetary Sciences, California Institute of Technology, Pasadena, California 91125, USA*
[3]*Lundin Norway AS, Lysaker 1366, Norway*
[4]*Department of Geology, University of Tartu, Tartu 50411, Estonia*

MATERIALS

The following photographs show calcite spar-native sulfur nodules that were sampled and analyzed in this study. The nodules range in size from <1 to >5 cm in diameter. Only nodules containing calcite spar or calcite spar and native sulfur were sampled – nodules containing only native sulfur were not studied. To produce material for stable isotope ratio analyses, small holes were drilled directly into the ~4 cm wide drill core (Figures S1 – S10). 200 µm polished 'thick' sections for geochronological analyses were prepared from 2.5 cm 'plugs' drilled directly out of the drill core.
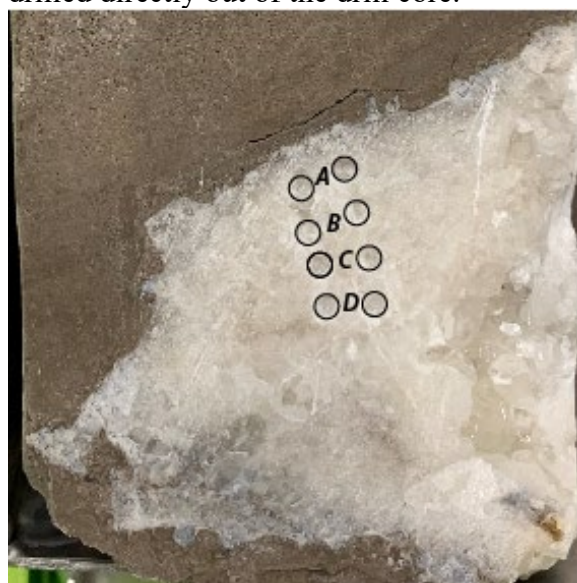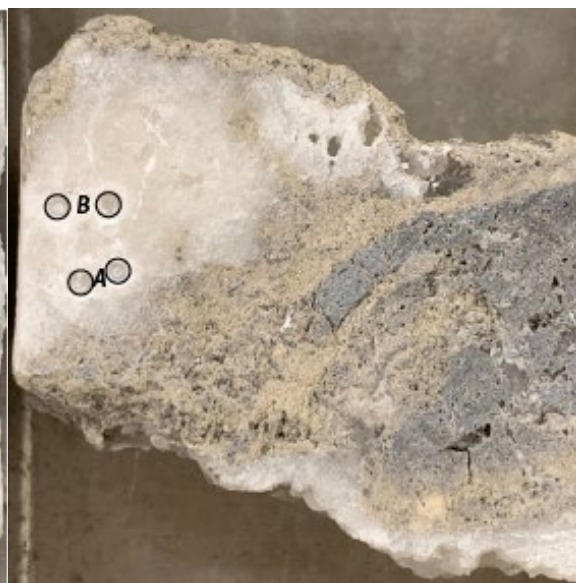

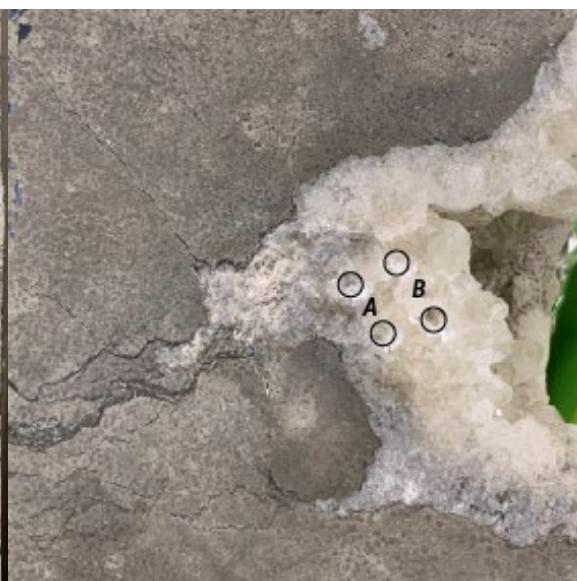***Figure S1.*** Sample 20.67   ***Figure S2.*** Sample 25.74

Figure S3. Sample 33.12

Figure S4. Sample 33.73

Figure S5. Sample 39.72

Figure S6. Sample 40.32

Figure S7. Sample 51.06

Figure S8. Sample 51.22

Figure S9. Sample 52.47   **Figure S10.** Sample 54.46

METHODS
XRF Element Mapping
Qualitative X-ray Fluorescence (µXRF) element maps were made using a Bruker M4 Tornado at Norges Teknisk-Naturvitenskapelige Universitet (NTNU; Trondheim, Norway) equipped with a silver X-Ray source and two silicon drift detectors. Analyses were conducted at 50 kV accelerating voltage and 600 µA, with an acquisition time of 2 ms/pixel. The distance between each pixel was 25 µm, and the analytical spot size was 20 µm. Mapping was conducted under a vacuum of 20 mbar. To reduce 'noise' in the output images, a 3-pixel averaging filter was applied. The element counts are not calibrated, and element maps should only be assessed individually.

LA ICP MS Element Mapping
Trace element mapping was carried out using a Teledyne-Cetac Analyte Excite 193 nm excimer laser ablation (LA) system connected to an Agilent 8900 inductively coupled plasma mass spectrometer (ICP MS) at the Geological Survey of Norway. A 35 µm square laser beam was rastered over areas of several mm^2 in each thin section, ablating lines left-to-right, and with 1 µm overlap between lines to avoid unablated gaps. Ablations were carried out in a He atmosphere within a two-volume laser cell, and ablated material was transported in a He carrier gas and mixed with Ar just before entering the plasma torch. The following analytes were measured sequentially with 6 ms dwell times on a secondary electron multiplier: ^{24}Mg, ^{27}Al, ^{29}Si, ^{31}P, ^{43}Ca, ^{49}Ti, ^{55}Mn, ^{56}Fe, ^{88}Sr, ^{89}Y, ^{139}La, ^{140}Ce, ^{141}Pr, ^{146}Nd, ^{147}Sm, ^{153}Eu, ^{157}Gd, ^{165}Ho, ^{206}Pb, ^{208}Pb, ^{232}Th, and ^{238}U. These elements were chosen to monitor for carbonate and detrital content, REE+Y element distributions, and variations in U-Pb systematics within the samples.

      The NIST 612 reference glass was used as a calibration standard and was measured between every 8 sample lines. The BHVO-2G reference glass was also measured several times in each sequence to evaluate data accuracy. Both reference glasses were analyzed by rastering over lines (~30-45 s for NIST 612 and ~30 s for BHVO-2G) with the same parameters used on the samples. Pauses of 8 s allowed signal washout between lines to avoid carryover of signal between measurements of sample lines and standards. Detailed instrument parameters are presented in Table S1.

Data were reduced using a customized version of the 'Trace Elements' data reduction scheme in Iolite v. 4.3.12 (Paton et al., 2011). On-peak baselines were subtracted from the signal on each mass. ^{43}Ca was used as an internal elemental standard (assuming 40 wt% Ca for the calcite) to account for differences in ablation yield, aerosol transport, etc. between the different sample and standard matrices. NIST 612 was used as a primary standard to calibrate ratios in sensitivity between each analyte and ^{43}Ca. Trace element maps were produced using the 'Create Image from Selections' tool in Iolite, with color scales chosen manually to maximize detail in minerals of interest.

The use of an appropriate calibration standard and internal elemental standard should, in theory, permit the accurate quantification of elemental concentrations. However, there are several challenges to quantification that are relevant to the trace element mapping of carbonate. Firstly, NIST 612 reference glass is not matrix-matched to carbonate samples. Secondly, accurate quantification relies on a known concentration of an internal elemental standard. For an area composed of pure calcite or aragonite, for example, a Ca concentration can be assumed based on stoichiometry of $CaCO_3$. However, if the carbonate phases are solid solutions with dolomite or other components, and 40 wt% Ca is assumed, this will lead to biases in the quantified elemental concentrations (and similarly for other minerals). Consequently, the maps are treated as only semi-quantitative results.

Table S1. Instrument parameters for LA ICP MS element mapping.

Agilent 8900 ICP MS	
Forward Power (W):	1150
Coolant Gas (5.0 purity Ar; L/min):	15.0
Auxiliary Gas (5.0 purity Ar; L/min):	0.9
"Nebulizer Gas" (5.0 purity Ar; L/min):	0.83
Analytes:	^{24}Mg, ^{27}Al, ^{29}Si, ^{31}P, ^{43}Ca,^{49}Ti, ^{55}Mn,^{56}Fe, ^{88}Sr, ^{89}Y, ^{139}La, ^{140}Ce, ^{141}Pr, ^{146}Nd, ^{147}Sm, ^{153}Eu, ^{157}Gd, ^{165}Ho, ^{206}Pb, ^{208}Pb, ^{232}Th, ^{238}U
Dwell Time (ms):	6
Duty Cycle (s):	0.1702
Analyte Excite LA Module	
Beam Diameter (μm):	35
Fluence (J/cm^2):	3.0
Repetition Rate (Hz):	10
Scan speed (μm/s):	20
He (5.0 purity) carrier gas into cell (L/min):	0.50
He (5.0 purity) carrier gas into laser arm (L/min):	0.30
Washout time between lines (s)	8

U-Pb Isotope Analyses

Uranium-lead isotopic analyses were done over four analytical sessions using a Teledyne-Cetac Analyte Excite 193 nm excimer laser ablation system connected to a Nu Instruments Plasma 3 multicollector (MC) ICP-MS at the Geological Survey of Norway. Thirty-second ablations were preceded by 20 s baselines and followed by 5 s washouts. ^{202}Hg, ^{204}Pb, and ^{204}Hg were measured on secondary electron multipliers, ^{206}Pb and ^{207}Pb were measured on Daly detectors, and ^{232}Th and ^{238}U were measured on Faraday cups with 1011-W resistors. ^{208}Pb was incident on a secondary electron multiplier but was deflected away to prevent tripping the ion counters when encountering large common-Pb signals. Detailed laser and MC ICP-MS instrument parameters are shown in Table S2.

Measurements of the reference materials NIST 614, UCSB 436, WC-1 calcite (Roberts et al., 2017), White Pine, and ASH-15 (Nuriel et al., 2021) were conducted at the beginning and end of each sequence, as well as between every 6 sample measurements.

Data were reduced using the "VizualAge UComPbine" data reduction scheme (Chew et al., 2014) in Iolite 4. On-peak baselines were fitted with an 'automatic spline' and subtracted from the signal on each channel. The first 3 s and last 3 s of signal were trimmed from each measurement. Measurements of NIST 614 were fitted with automatic splines and were used to correct for drift in the ^{238}U/^{206}Pb ratio, as well as to normalize the ^{207}Pb/^{206}Pb ratios. Due to assumed differences in elemental fractionation behavior between glass and carbonate matrices, no downhole U-Pb fractionation correction was performed, necessitating the use of data from the same interval for each measurement (i.e., with 3s and 3 s trimmed from the beginning and end, respectively). Further normalization and uncertainty propagation were performed offline. Also due to differences in elemental fractionation behavior between glass and carbonate matrices, drift-corrected U/Pb ratios for the calcite measurements required normalization to a reference calcite. The ^{238}U/^{206}Pb of individual analyses were normalized using the discord lower-intercept date in each sequence relative to a reference age of 11.1Ma for the UCSB 436 reference calcite. An additional 2.5% and 1% were quadratically added the ^{238}U/^{206}Pb and ^{207}Pb/^{206}Pb ratios, respectively, for each measurement.

Concordia diagrams and ages were generated with IsoplotR (Vermeesch, 2018). The dates reported here are unanchored discordia lower-intercept dates, and the uncertainties are the studentized 95% confidence interval scaled by the square root of the MSWD (if MSWD > 1) for overdispersed data. Results for the secondary calcite standards measured with the samples in this contract are as follows:

- ASH-15
  - **Nuriel et al. (2021):** 2.965 ± 0.011 Ma
  - **This study:** 2.998 ± 0.034 Ma, n = 44, MSWD = 1.9, $^{207}Pb/^{206}Pb_c$ = 0.8194 ± 0.003
- White Pine
  - **Kylander-Clark (Personal Communications):** 13.0 Ma
  - **This study:** 13.155 ± 0.124 Ma, n = 44, MSWD = 2, $^{207}Pb/^{206}Pb_c$ = 0.6996 ± 0.0043
- WC-1
  - **Roberts et al. (2017):** 254.4 ± 6.4 Ma
  - **This study:** 264.87 ± 5.42 Ma, n = 44, MSWD = 12, $^{207}Pb/^{206}Pb_c$ = 0.85.

The ages reproduced for the secondary standards ASH-15 and White Pine are accurate to within 2%. The large uncertainty in the age for WC-1 is likely due to heterogeneity of some parts of standards, which has been reported by others (Guillong et al., 2020). The lower-intercept ages for ASH-15 and White Pine are more precise (~1.5%). To account for systematic uncertainties, for example bias in the age results for the secondary reference calcites and uncertainties in the age of the reference calcites, an additional blanket uncertainty of 2.5% was quadratically added to statistical uncertainties of the dates reported for the samples.

The standard reference materials have U contents of 0.9 ppm (NIST 614; Hollocher and Ruiz, 1995), 1 ppm (ASH-15; Nuriel et al., 2021), and 3.7 ppm (WC-1; Roberts et al., 2017), similar to the U contents of the studied samples (typically ranging from 1 to 6 ppm).

Table S2. Instrument parameters for U-Pb analyses.

Nu Instruments Plasma 3 MC ICP MS	
Forward Power (W):	1300
Coolant Gas (5.0 purity Ar; L/min):	13.5
Auxiliary Gas (5.0 purity Ar; L/min):	0.9
"Mix Gas" (5.0 purity Ar; L/min):	1.07
Monitored Masses:	^{202}Hg, ^{204}Hg, ^{204}Pb, ^{206}Pb, ^{207}Pb, ^{232}Th, ^{238}U
Integration Period (s):	0.1
Analyte Excite LA Module	
Beam Diameter (μm):	85
Fluence (J/cm^2):	3.0
Repetition Rate (Hz):	10
He (5.0 purity) carrier gas into cell (L/min):	0.131-0.144
He (5.0 purity) carrier gas into laser arm (L/min):	0.09
Baseline, ablation, and washout times, respectively (s)	20, 30, 5

Carbon, Oxygen, and 'Clumped' Isotope Ratio Analyses

Carbon and Oxygen isotope ratio analyses ($\delta^{13}C$ and $\delta^{18}O$, respectively) were conducted at the University of Tartu, Estonia, and the California Institute of Technology, U.S.A. At the University of Tartu, analyses were conducted using a GasBench II sample preparation device coupled to a Thermo Scientific Delta V Advantage isotope ratio mass spectrometer (IRMS). Samples were dissolved in >99% phosphoric acid with a reaction time of >8 hours to ensure complete dissolution of carbonate minerals. Analyses were calibrated against the standard reference materials NBS 18, IAEA 603, LSVEC, and IAEA 611, with 1σ uncertainties smaller than ± 0.2‰.

Analyses of $\delta^{13}C$, $\delta^{18}O$, and Δ_{47} at the California Institute of Technology were carried out using previously established methods (Ghosh et al., 2006; Huntington et al., 2009; Passey et al., 2010; Dennis and Schrag, 2010). Seven to ten mg of samples were drilled directly from drill core 7029/03-U-02 and digested with phosphoric acid at 90°C to produce CO_2. The CO_2 was separated from H_2O, trace organics and other polar contaminants by dry ice/ethanol and liquid nitrogen traps as well as entraining the CO_2 in He and passing over a Porapak Q 120/80 mesh column held at -20 °C. The resulting CO_2 was again purified from He using dry ice/ethanol and nitrogen traps and expanded into the bellows of the IRMS. The evolved CO_2 was analyzed in a dual inlet Finnigan MAT-253 IRMS with the simultaneous collection of ion beams corresponding to masses 44-48 to obtain Δ_{47}, Δ_{48}, $\delta^{13}C$ and $\delta^{18}O$ values. The mass 47 beam is composed of $^{17}O^{13}C^{17}O$, $^{17}O^{12}C^{18}O$ and predominantly $^{18}O^{13}C^{16}O$ and we define R_{47} as the abundance of mass 47 isotopologues divided by the mass 44 isotopologue:

$$R_{47} = [^{17}O^{13}C^{17}O + {}^{17}O^{12}C^{18}O + {}^{18}O^{13}C^{16}O]/[^{16}O^{12}C^{16}O]$$

Δ_{47} is reported relative to a stochastic distribution of isotopologues for the same bulk isotopic composition:

$$\Delta_{47}=(((R_{47measured}/R_{47stochastic})-1)-((R_{46measured}/R_{46stochastic})-1)-((R_{45measured}/R_{45stochastic})-1))*1000$$

Mass 48 was monitored to detect any hydrocarbon contamination. All samples fell on the Δ_{48}-line derived from heated and equilibrated gases within 3σ. Measurements of each gas were done at 16 V of mass 44 and consisted of 8 acquisitions, each of which involved 7 cycles of sample-standard comparison with an ion integration time of 26 s per cycle. Internal standard errors for Δ_{47} ranged from 0.01-0.02‰. Reported errors are the propagated errors of the internal error, heated gas line error and Δ_{47}-temperature calibration.

$\delta^{13}C$ and $\delta^{18}O$ values of samples and standards were calculated from raw ion currents on masses 44, 45, and 46 of sample and working gases using the 'Brand' parameters reported in Brand et al. (2010). The acid digestion fractionation factors for aragonite and calcite have been calculated between 25 to 75°C, and we extrapolate these values to 90°C and use them in our calculations (Kim et al., 2007). Raw Δ_{47} values were then calculated from the difference in R_{47} relative to the reference gas and the newly derived $\delta^{13}C$ and $\delta^{18}O$ values of the derived sample gas. The Δ_{47} raw data was corrected for instrument nonlinearity and scale compression (Huntington et al., 2009; Passey et al., 2010). Several heated and equilibrated gases of various bulk isotopic compositions were run during the session. These gases were used to convert measurements into the interlaboratory absolute reference frame (Dennis et al., 2011). Reported values are based on one analyses per sample (i.e., no replicates).

Burial History Modelling

Basin modelling was performed using the Trinity software from ZetaWare Inc. Regional depth maps, based on seismic interpretations, were used as the input for thermal modelling,

and borehole temperature data was extracted from exploration wells in the area. The burial and temperature history was constructed using regional depth maps from regional seismic interpretation done by Lundin Energy Norway. A constant geothermal gradient of 35°C/km was used, calculated from exploration well data available from the Norwegian Petroleum Directorate fact pages (npd.no). Net erosion was estimated from vitrinite reflection versus depth trends. A one-dimensional temperature-time model was constructed to represent the thermal evolution of the Ørn Formation. The main uncertainties in this approach are the maximum burial depths of the stratigraphy and variations in subsurface paleo-temperatures through time. Therefore, results from the thermal modelling should be treated more as approximations of the temperatures and event timing, rather than accurate statements of the temperatures.

Burial history modelling was conducted entirely independent of the U-Pb dating and clumped isotope paleothermometry carried out as part of this study – no geochemical results from this study were used to inform the burial history model.

RESULTS
XRF Element Maps
Sample 32.65
This sample consists largely of dolomite (medium bright in Ca and Mg), with areas of native sulfur (bright in S) and small patches of calcite spar (bright in Ca).
Sample 27.31
This sample is approximately half dolomite (medium bright in Ca and Mg), with approximately 30% composed of calcite spar (bright in Ca), and 20% native sulfur (bright S) that infills void spaces between calcite spar.
Sample 16.50
This sample consists mostly of anhydrite (medium bright S and Ca), with small amounts of wispy, Fe-rich calcite micrite (bright in Ca).

Figure S11 (following page). XRF element maps for samples 32.65, 27.31, and 16.50 from well 7029/03-U-02. Selected areas from these samples were subsequently analysed for LA ICP MS element mapping and U-Pb isotope ratios.

| | 7129/3-U-2 32,65 | 7129/3-U-2 27,31 | 7129/3-U-2 16,50 |
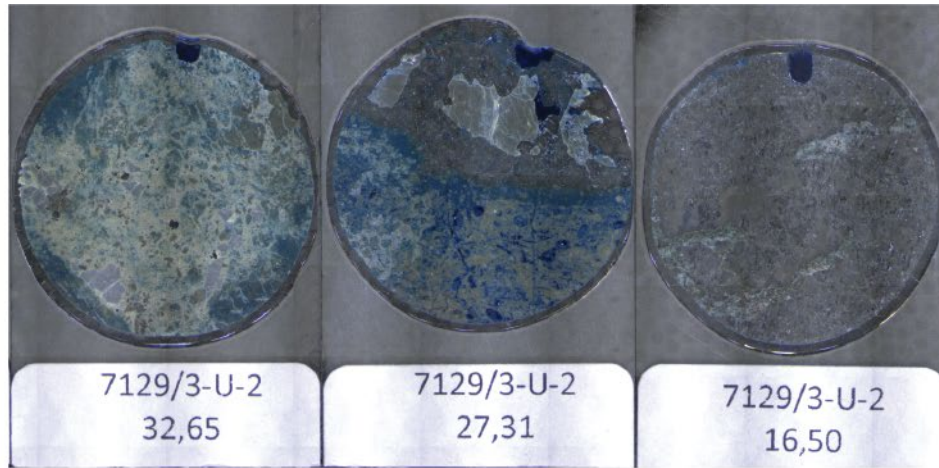
Al
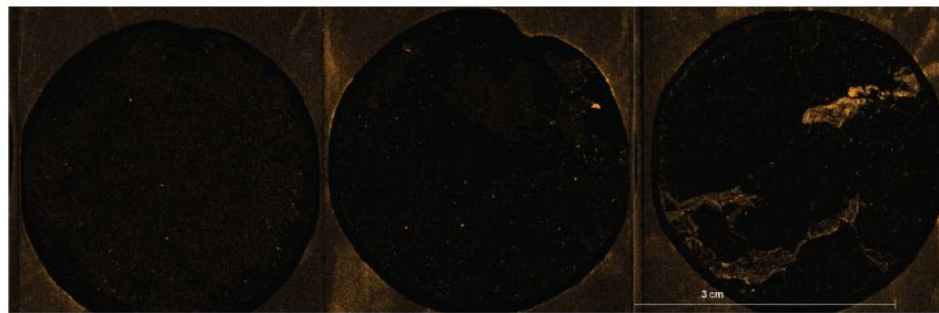
Ca
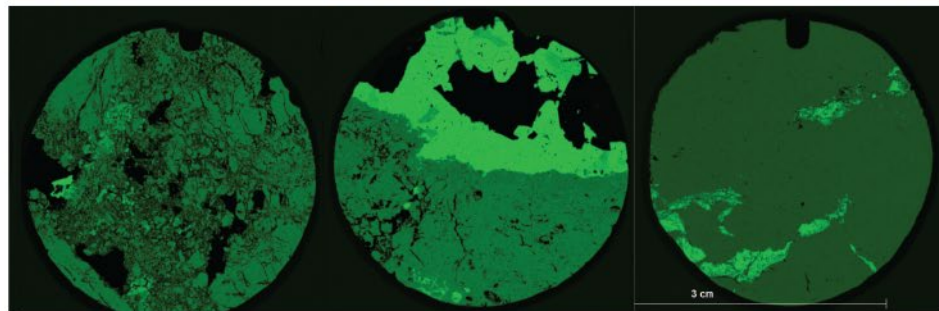
Fe
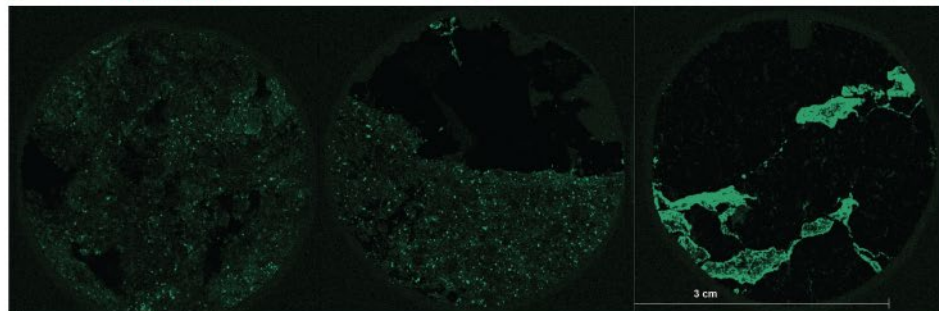
K
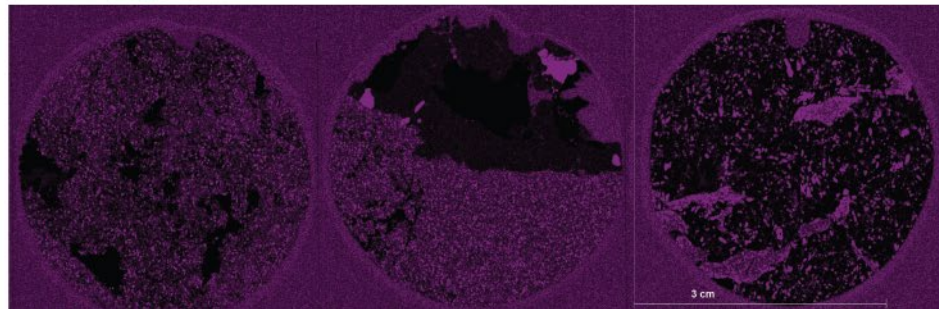
Mg
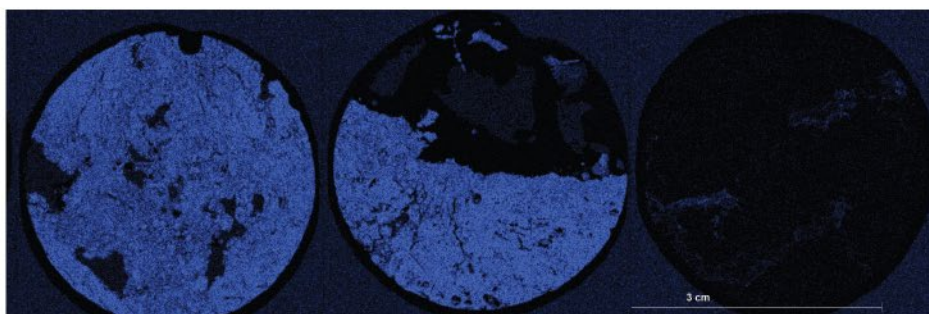
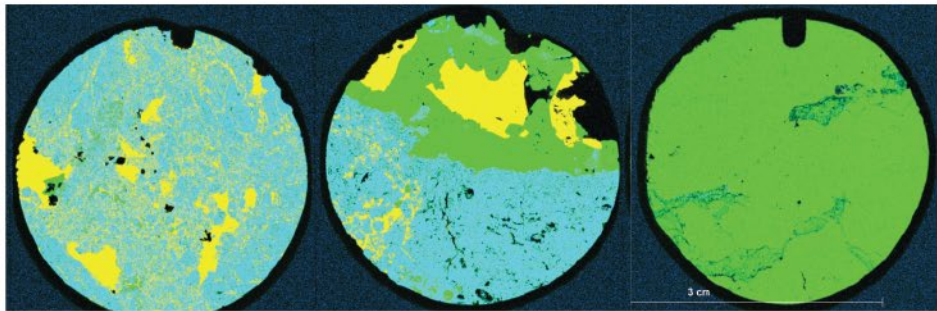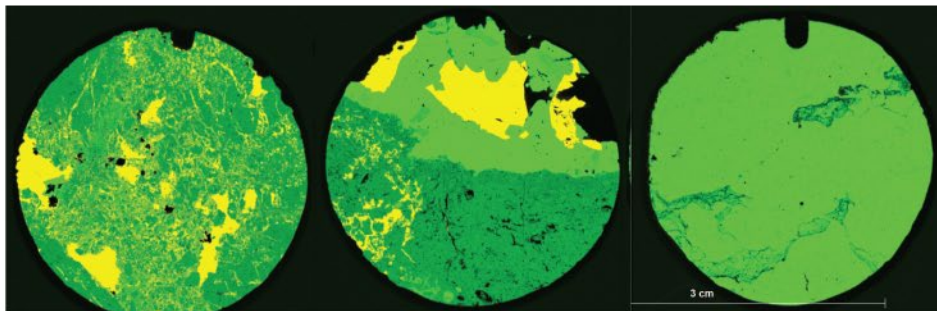**Mn**
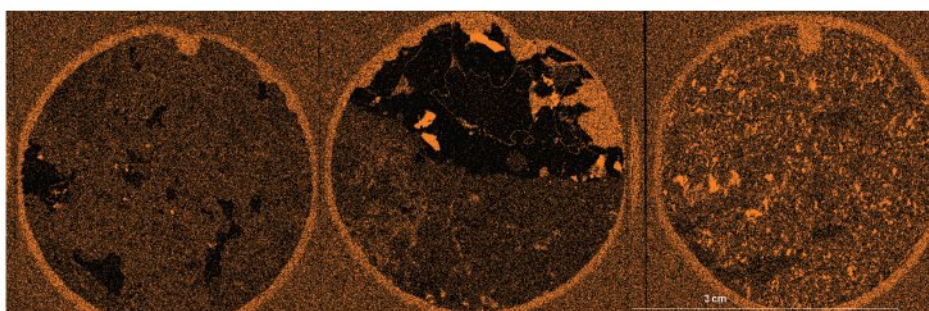
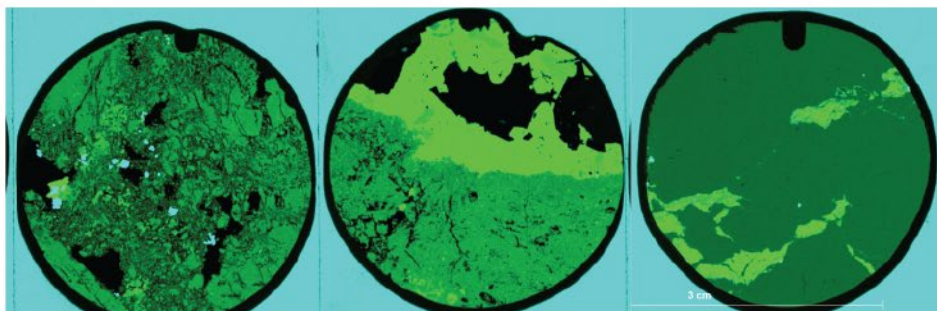**S**

Si
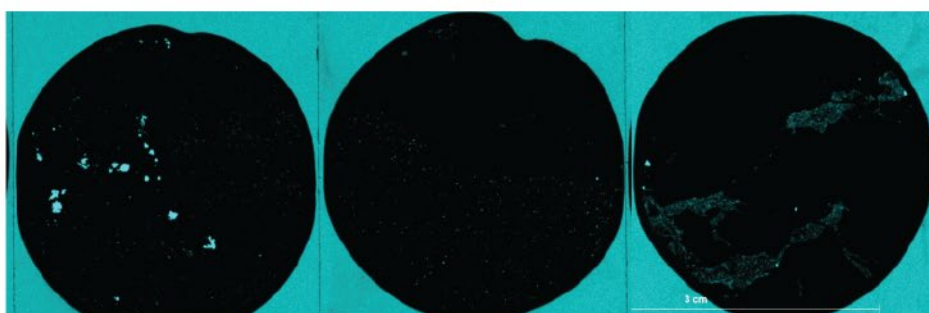
Al, Si
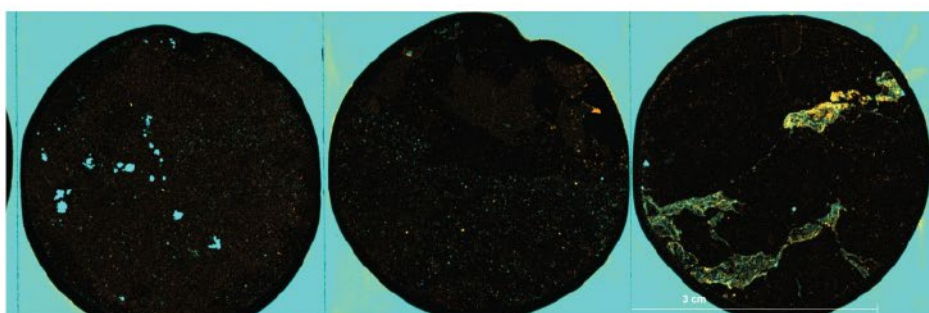
Ca, Mg
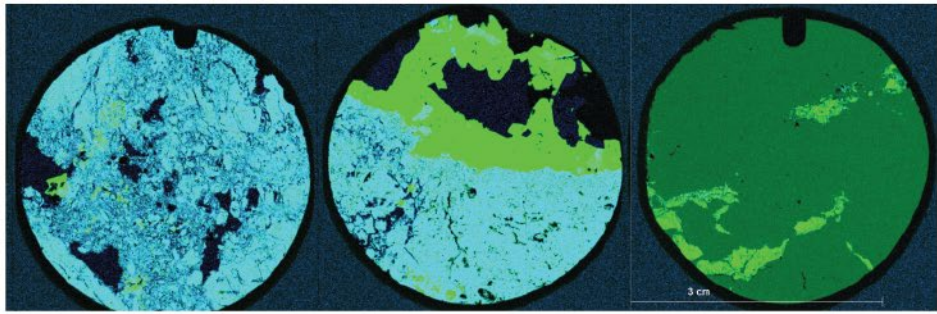
Ca, Mg, S

Ca, S

Ca, Si

LA ICP MS Element Maps

Based on the µXRF element maps, ca. 2 x 3 mm areas from each sample were selected for high resolution LA ICP MS element mapping. The generated LA ICP MS element maps were then used to guide spot placement for U-Pb isotope ratio analyses. Color scales were manually adjusted for each sample/element, and therefore cannot be used for comparison between samples.

Sample 16.50
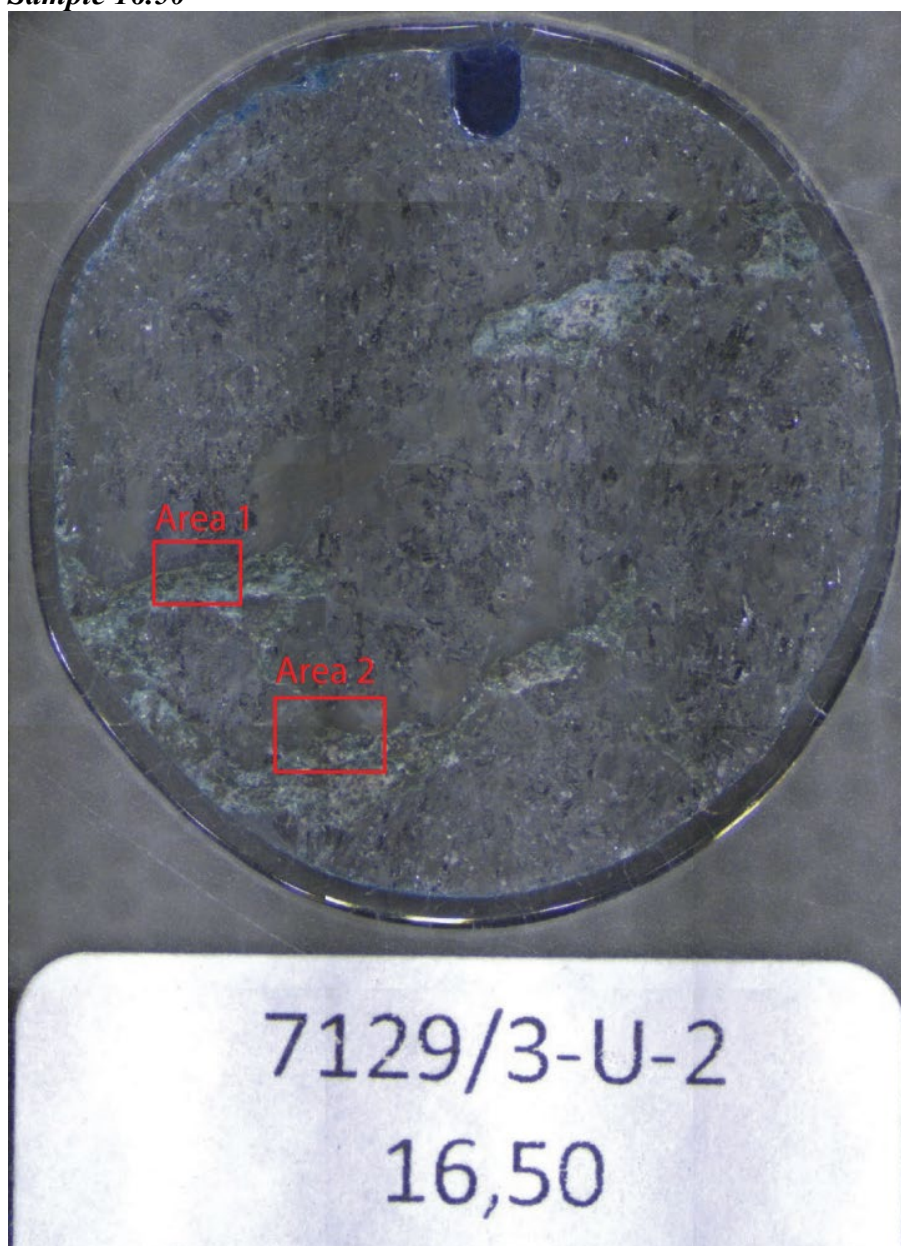
Figure S12. Areas of sample 16.50 selected for LA ICP MS element mapping.

Area 1 – Calcite micrite and anhydrite

Figure S12. Post-ablation photomicrograph of sample 16.50 area 1.
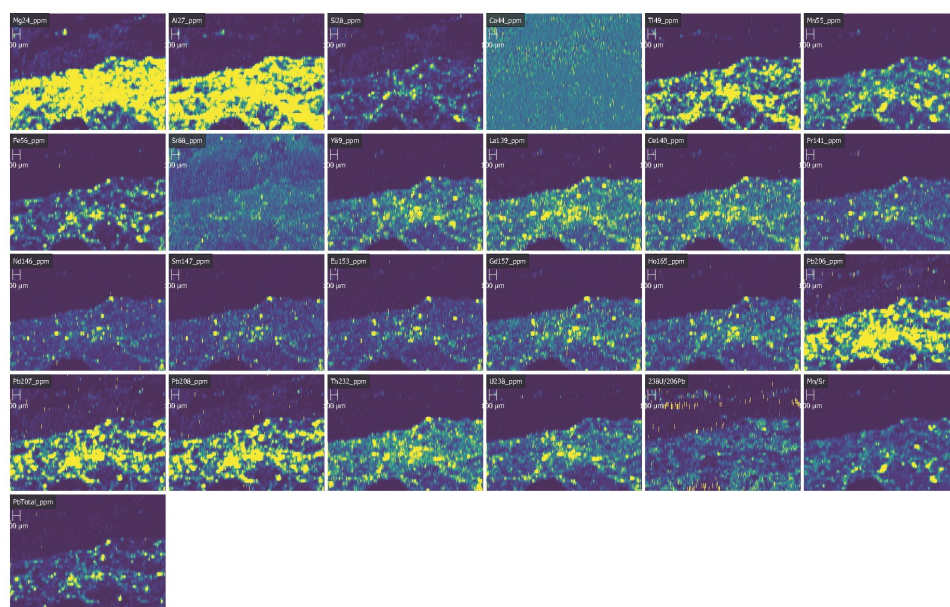
Figure S13. LA ICP MS element map of sample 16.50 area 1.

Area 2 – Calcite micrite and anhydrite
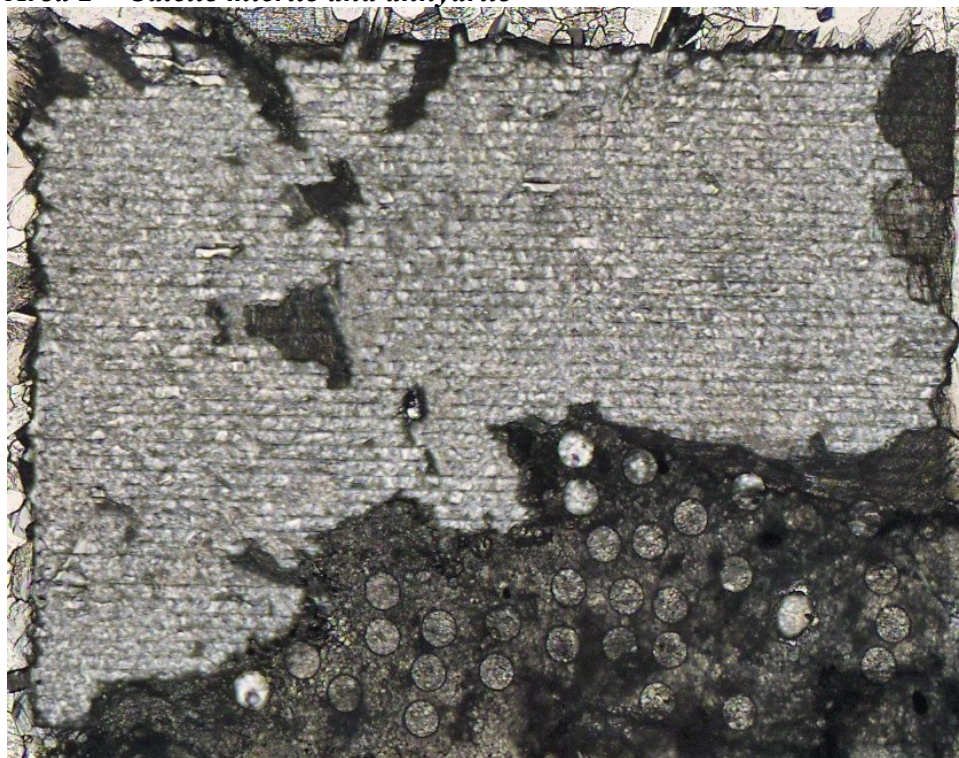
Figure S14. Post-ablation photomicrograph of sample 16.50 area 2.
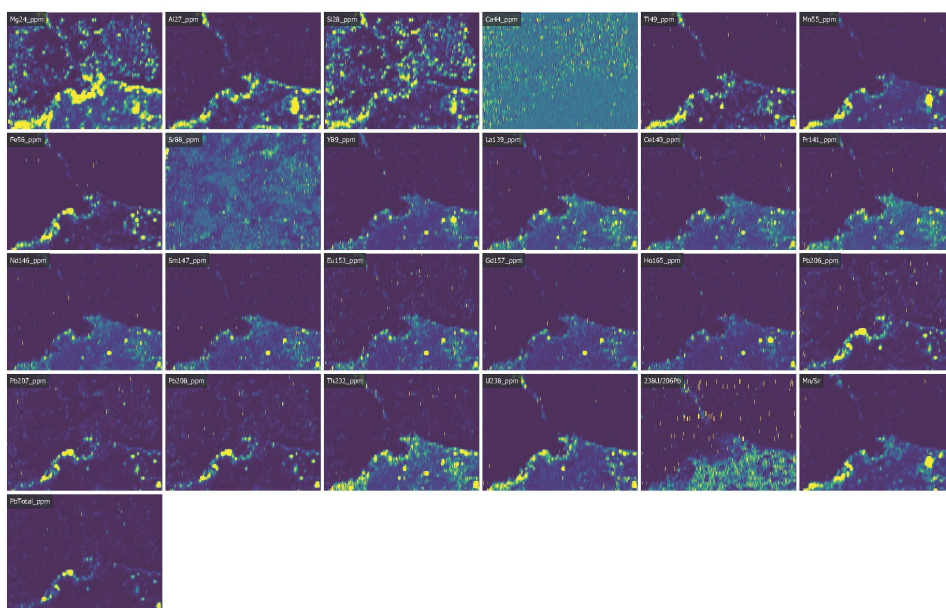
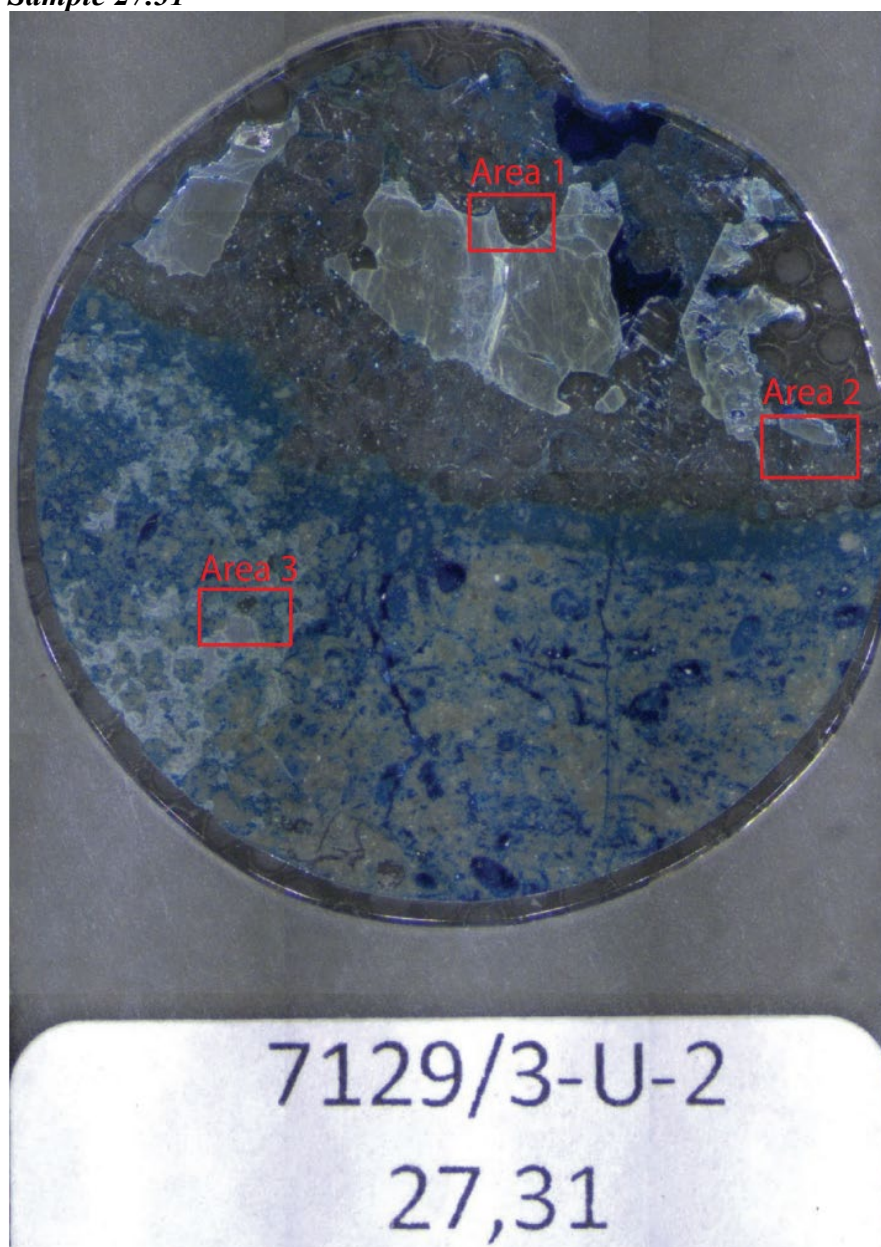**Figure S15.** LA ICP MS element map of sample 16.50 area 2.

Sample 27.31

Figure S16. Areas of sample 27.31 selected for LA ICP MS element mapping.

Area 1 – Calcite spar and native sulfur

Figure S17. Post-ablation photomicrograph of sample 27.31 area 1.
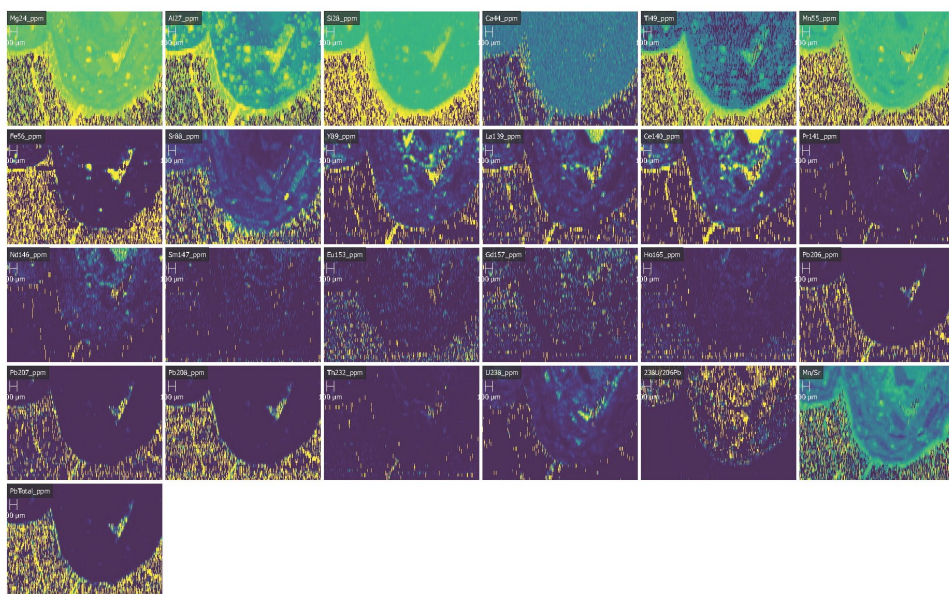
Figure S18. LA ICP MS element map of sample 27.31 area 1.
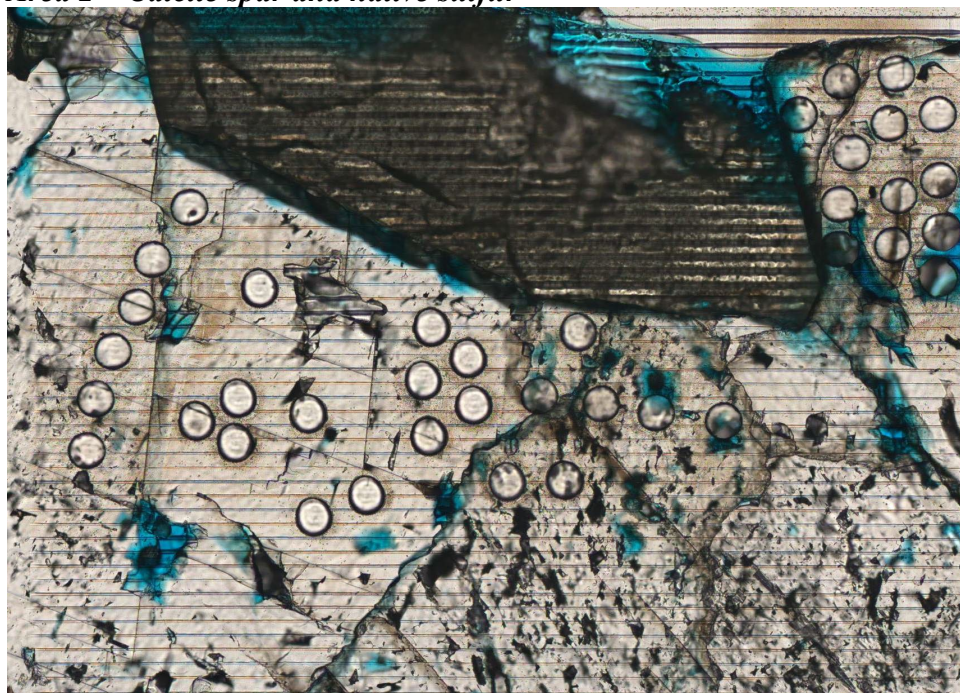
Area 2 – Calcite spar and native sulfur

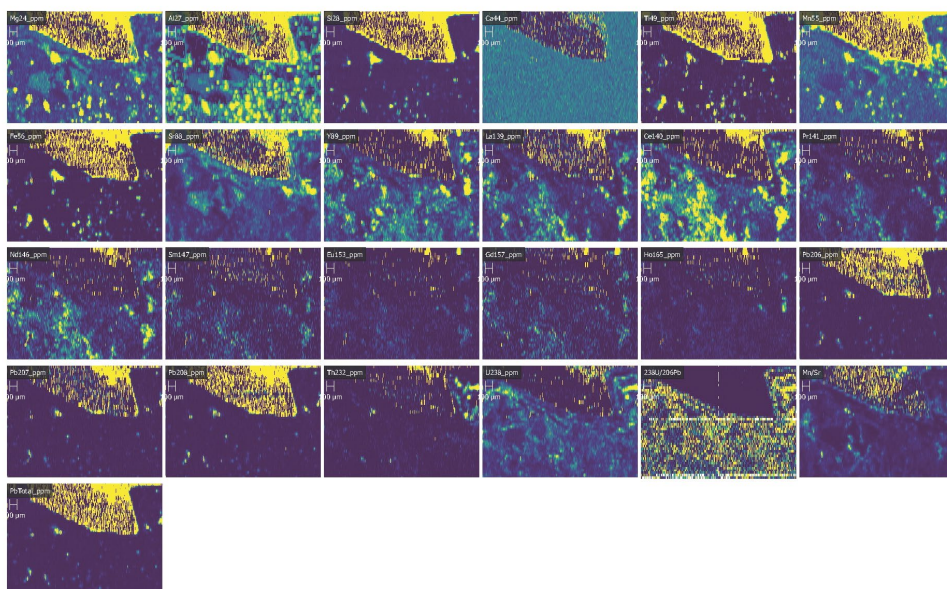**Figure S19.** Post-ablation photomicrograph of sample 27.31 area 2.

Figure S20. LA ICP MS element map of sample 27.31 area 2.
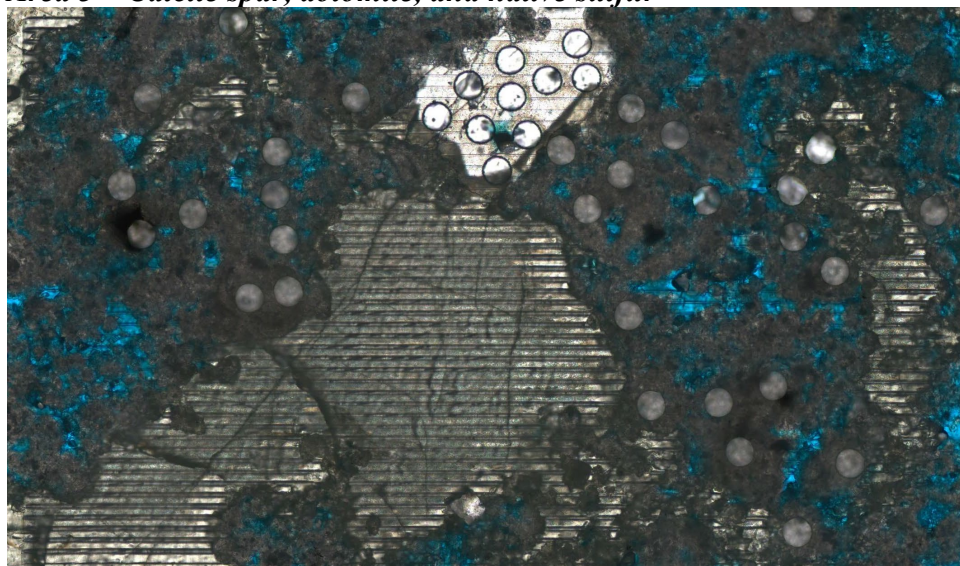
Area 3 – Calcite spar, dolomite, and native sulfur

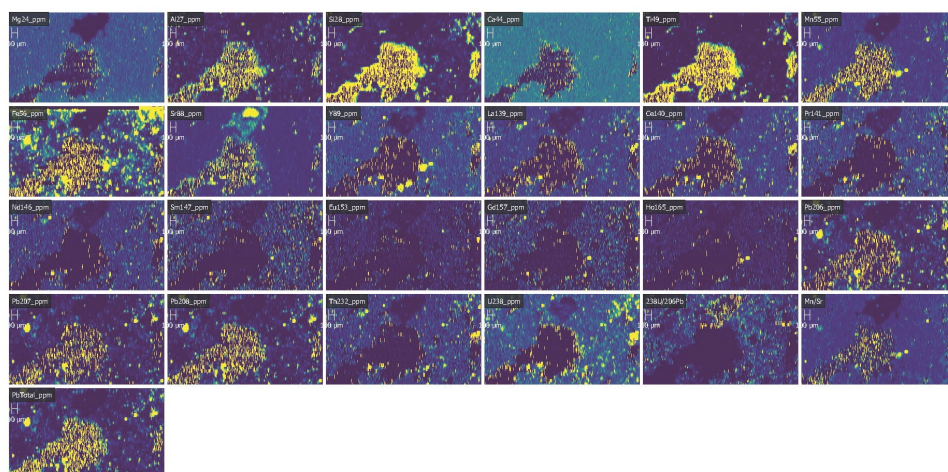***Figure S21.*** Post-ablation photomicrograph of sample 27.31 area 3.

Figure S22. LA ICP MS element map of sample 27.31 area 3.

Sample 32.65

Figure S23. Areas of sample 32.65 selected for LA ICP MS element mapping.

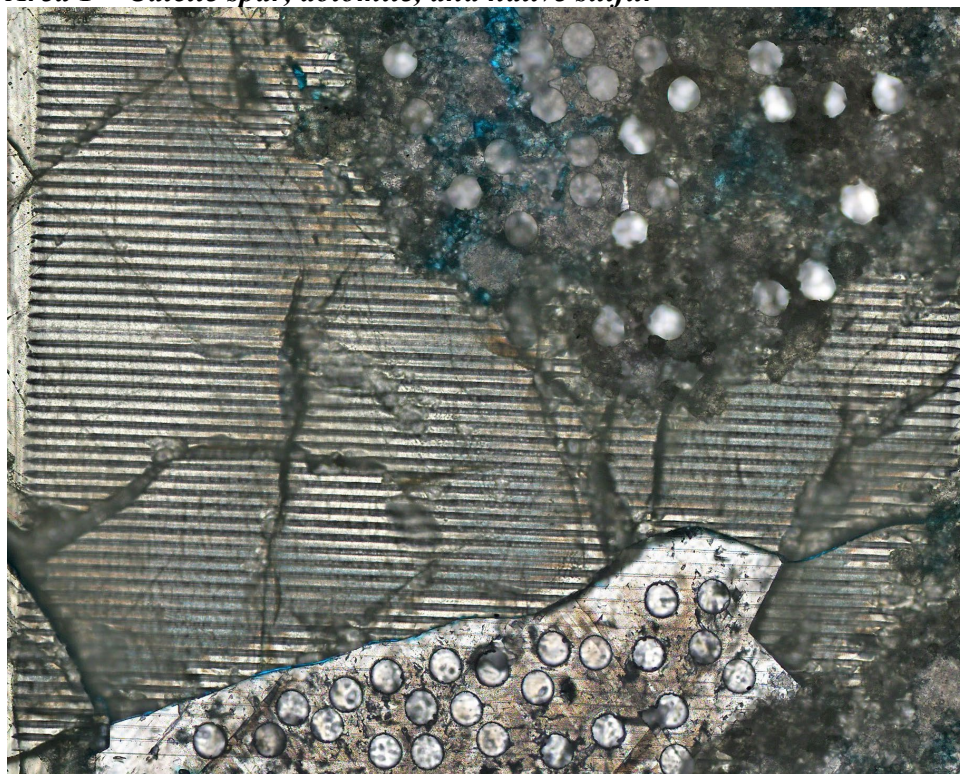*Area 1 – Calcite spar, dolomite, and native sulfur*

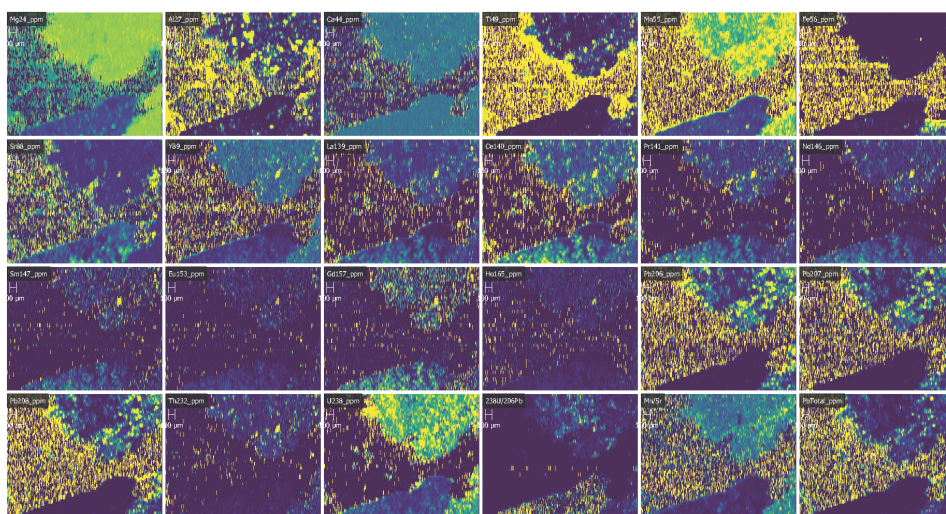**Figure S24.** Post-ablation photomicrograph of sample 32.65 area 1.

Figure S25. LA ICP MS element map of sample 32.65 area 1.
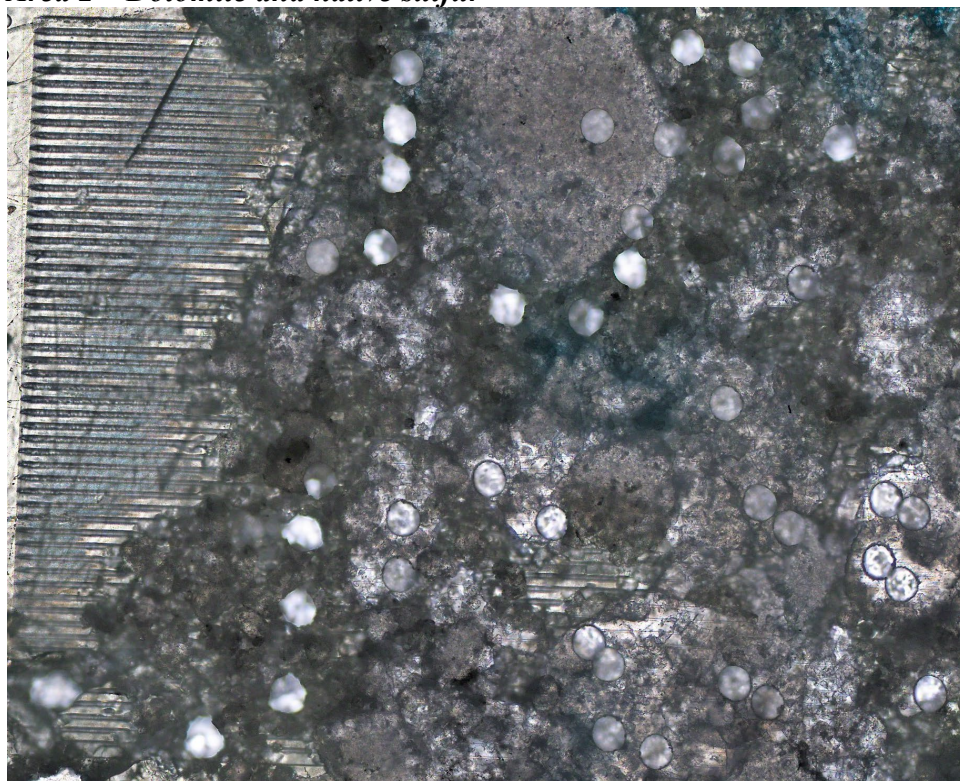
Area 2 – Dolomite and native sulfur

Figure S26. Post-ablation photomicrograph of sample 32.65 area 2.
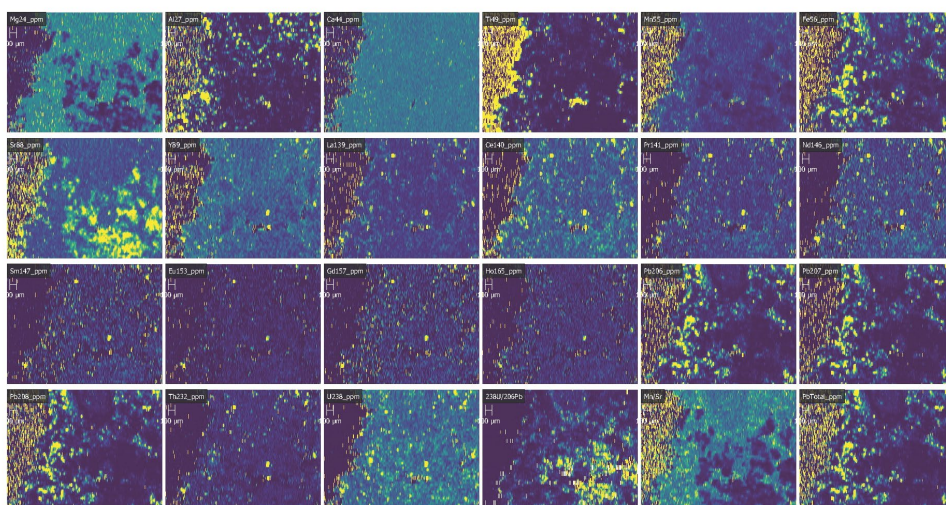

Figure S27. LA ICP MS element map of sample 32.65 area 2.

Mixing of different phases/age domains

Area 2 of Sample 32.65 consists of dolomitized host rock with clear 'patches' of calcite spar (Figure S26). Element mapping (Figure S27) shows that these patches of calcite spar contain relatively Mg-rich domains, likely representing a mixture of calcite spar and host rock dolomite. This is further supported by the U-Pb measurements for this sample (Figure S28), where analyses of the patchy calcite spar in Area 2 plot between the host rock dolomite from Areas 1 and 2, and the pure calcite spar from Area 1. Given these lines of evidence, all calcite spar U-Pb measurements from the calcite patches in Sample 32.65 Area 2 are considered unreliable for identifying calcite spar formation ages.
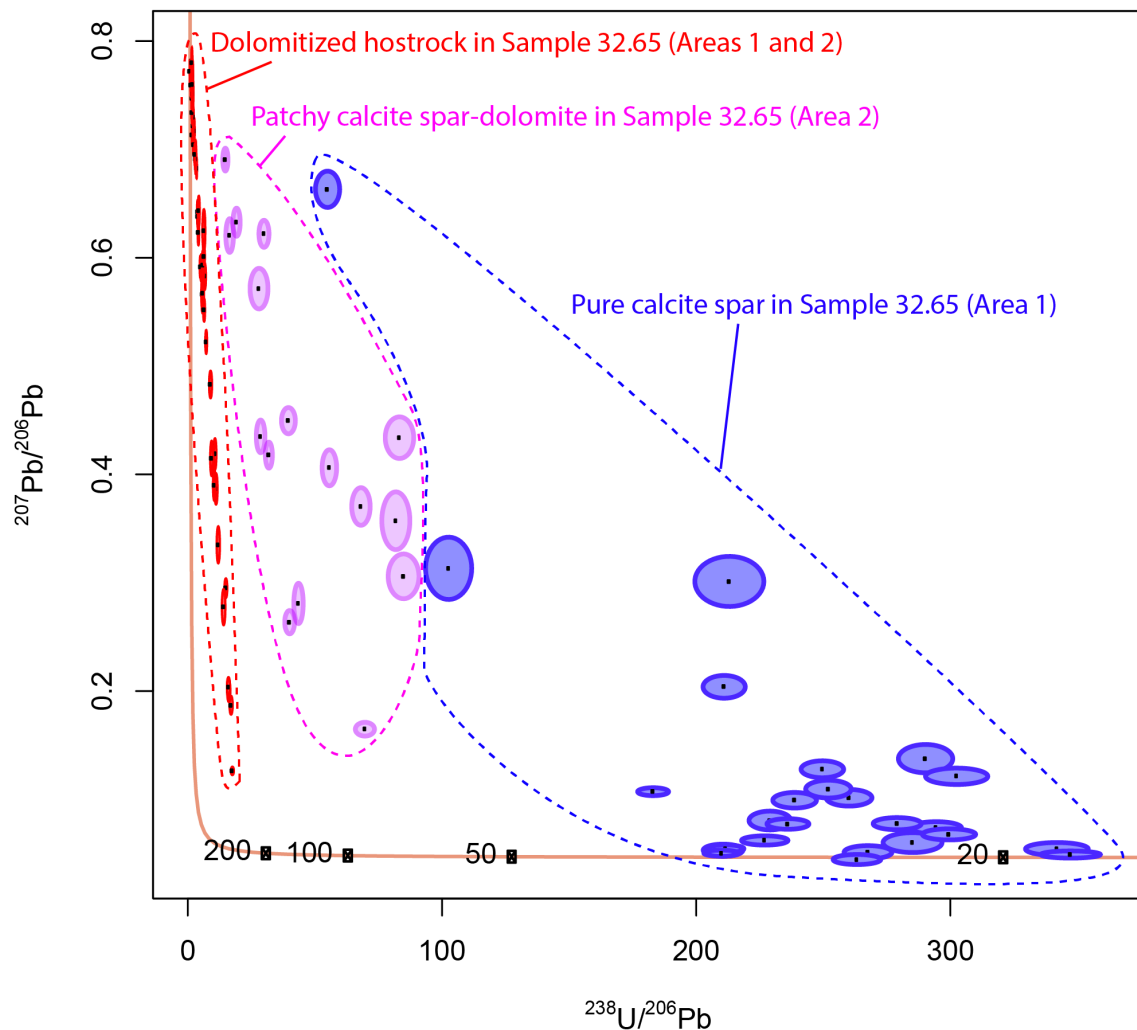
Figure S28. *U-Pb measurements from different phases of Sample 32.65 indicate that analyses of small calcite spar patches in Area 2 represent mixing between two different domains: dolomite host rock and pure calcite spar. Consequently, these geochronological data are not used for interpretation.*

'Younging' in direction of growth

One spar crystal studied in Area 1 of Sample 27.31 exhibits concentric trace element zonation (Figure S18). Ablation spots were placed in these zones to determine if the crystal is 'younging' in the direction of growth (toward the center of the nodule). The results (Figure S29) indicate that there is a general tendency for younger ages at the crystal edges (toward the nodule center), although there is overlap between the different regions, potentially due to mixing of different domains during ablation. A more detailed study of zoned calcite spar in these strata would be helpful for more robustly determining age-growth relationships for the calcite spar.
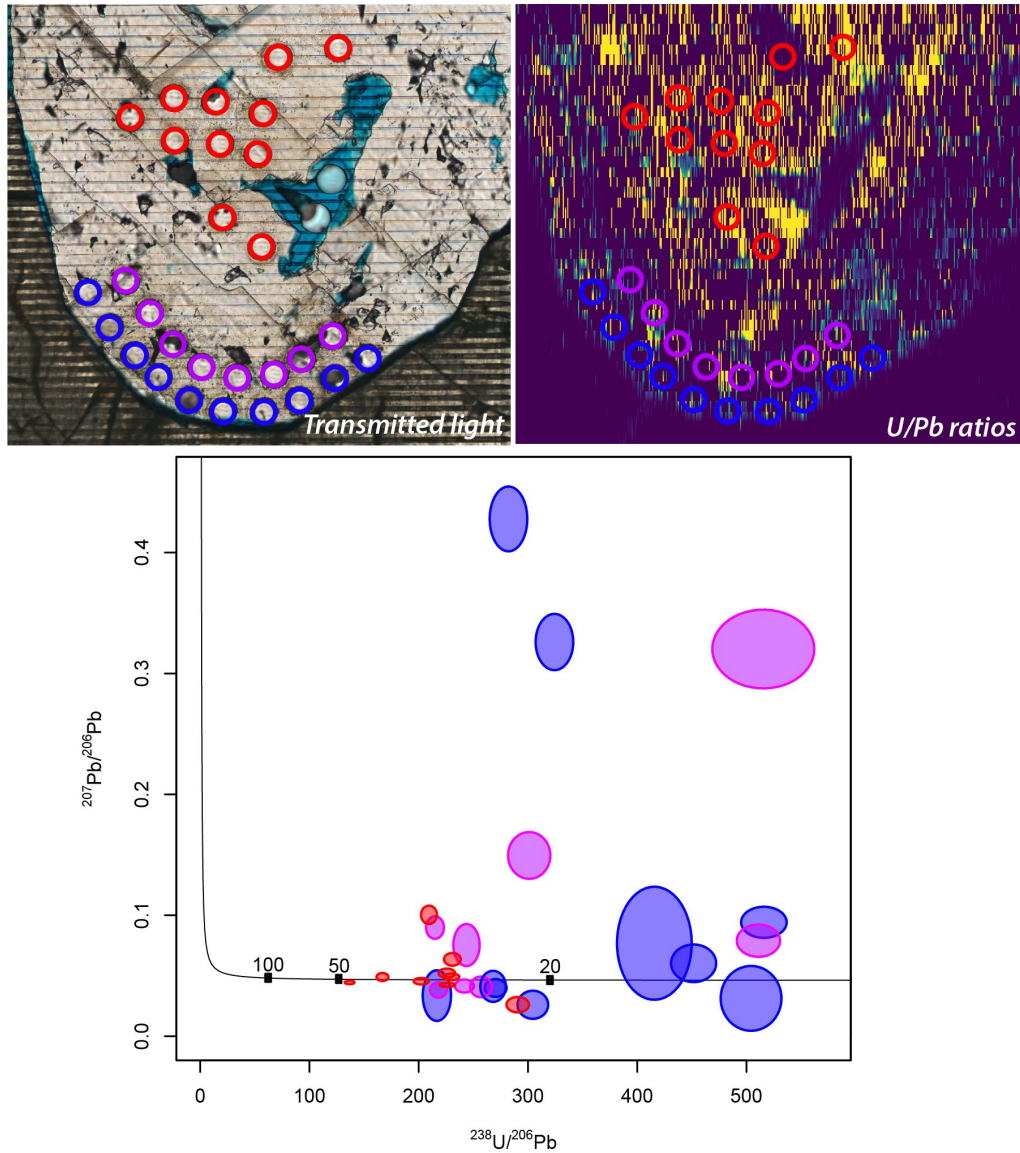
Figure S29. *Analyses in Area 1 of Sample 27.31 show a general tendency for the core of the calcite spar crystal to be older than the margins that have grown toward the center of the nodule (i.e., the spar toward the center of the nodule is younger than the spar toward the edge of the nodule). Color of datapoint corresponds to color of ablation spot indicated in photomicrograph/element map.*

Ablation depth

Ablation depth can be an important factor for calculating in-situ U/Pb ages. The average depth of ablation for calcite spar was $0.0295 \pm .004$ mm, compared to 0.0370 ± 0.016 mm ($\pm$ 2σ) for dolomite host rock. A shift toward older ages with deeper ablation craters (i.e., higher aspect ratios) has been noted by Guillong et al. (2020). The deeper ablation craters in the dolomite host rock, combined with the absence of a dolomite standard reference material for carbonate U/Pb geochronology. These analytical issues may contribute to uncertainties and explain the slightly older dolomite ages than expected based on biostratigraphy.

Reconstructed fluid $\delta^{18}O_{water}$ of the carbonates

A carbonate clumped isotope measurement provides a measure of the temperature of carbonate mineral crystallization in cases where the mineral formed at equilibrium. This

measure is independent of the mineral $\delta^{18}O$ value. When the two are combined, it allows one to independently calculate the $\delta^{18}O$ of the coexisting fluid, assuming the crystallization occurred at equilibrium. We calculate $\delta^{18}O_{fluid}$ values for the measured calcite spar and find that they vary from -5.1 to +4.5‰. Additionally, the calculated $\delta^{18}O_{fluid}$ values are strongly correlated with calculated precipitation temperatures. We believe there are two possible options to explain the observed variations in the $\delta^{18}O_{fluid}$. In the first option, the calcite spar may be precipitating from a fluid that has varying amounts of components characterized by low $\delta^{18}O_{fluid}$, likely a modified seawater or meteoric water, and high $\delta^{18}O_{fluid}$, likely a deeply sourced fluid (Taylor, 1974). In the second option, the calcite spar may be forming from fluids experiencing evolving $\delta^{18}O_{fluid}$ due to equilibration with the dolomite host rock under dynamic burial/exhumation regime with heavier $\delta^{18}O_{fluid}$ values reflecting fluid equilibration with the host rock at higher temperatures.
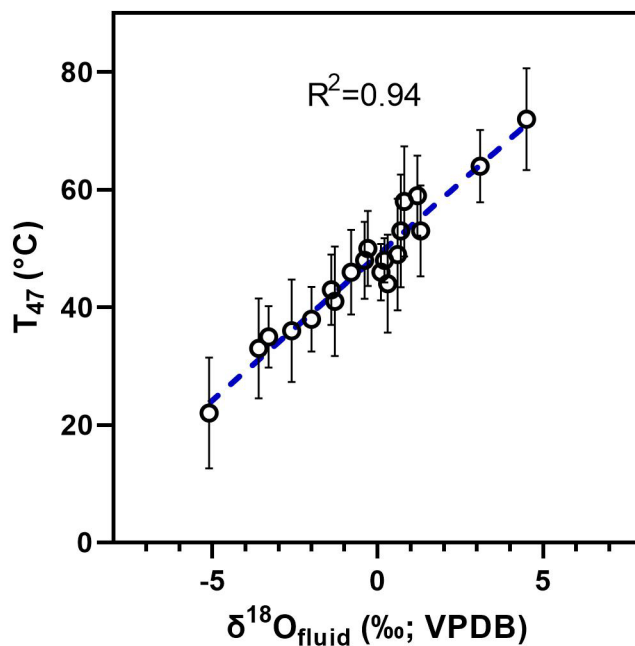

Figure S30. There is a stong relationship between precipitation temperature of calcite spar and calculated fluid $\delta^{18}O$ composition, which may represent spar precipitation from a fluid with varying proportions of seawater/meteoric/deeply sourced fluids, or evolving fluid $\delta^{18}O$ due to equilibration with the host rock dolomite under a varying temperature conditions of fluid equilibration.

Relationship between T_{47}, $\delta^{13}C$, and $\delta^{18}O$
There is no significant relationship between T_{47} and $\delta^{13}C$ or T_{47} and $\delta^{18}O$, with R^2 values of 0.20 and 0.09, respectively.
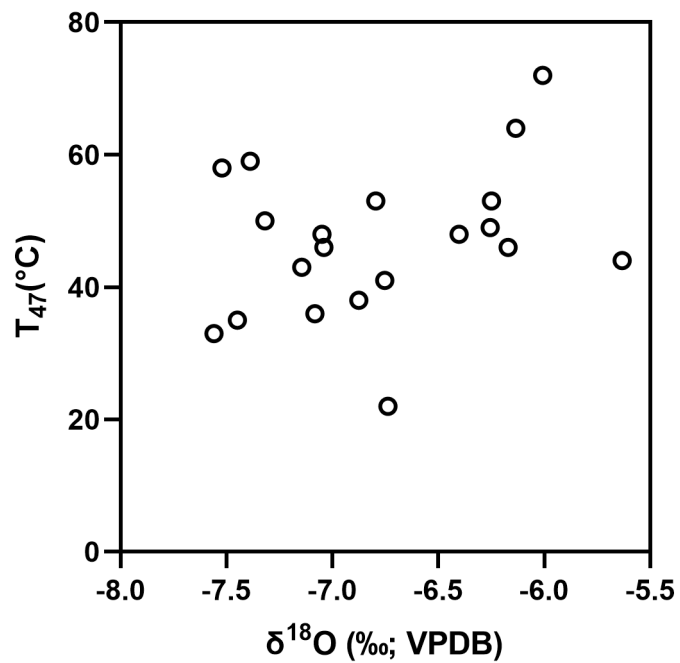
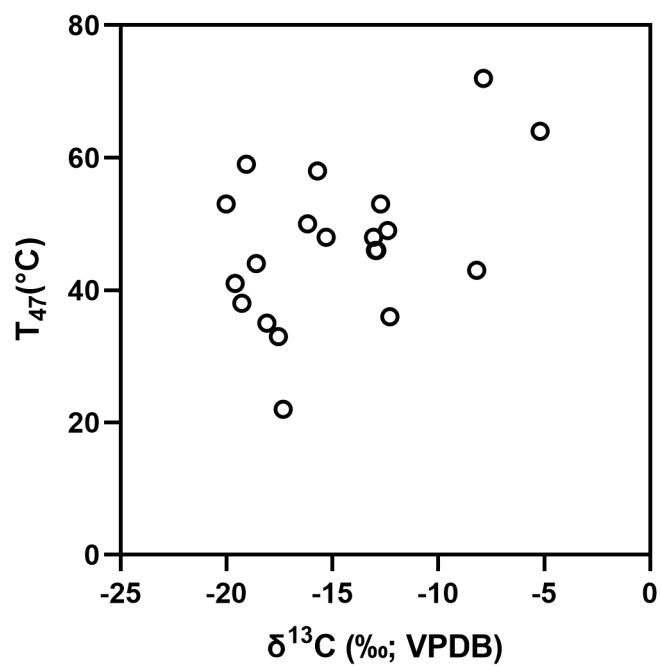***Figure S31.*** Crossplot of calculated T_{47} and $\delta^{18}O$ from calcite spar.

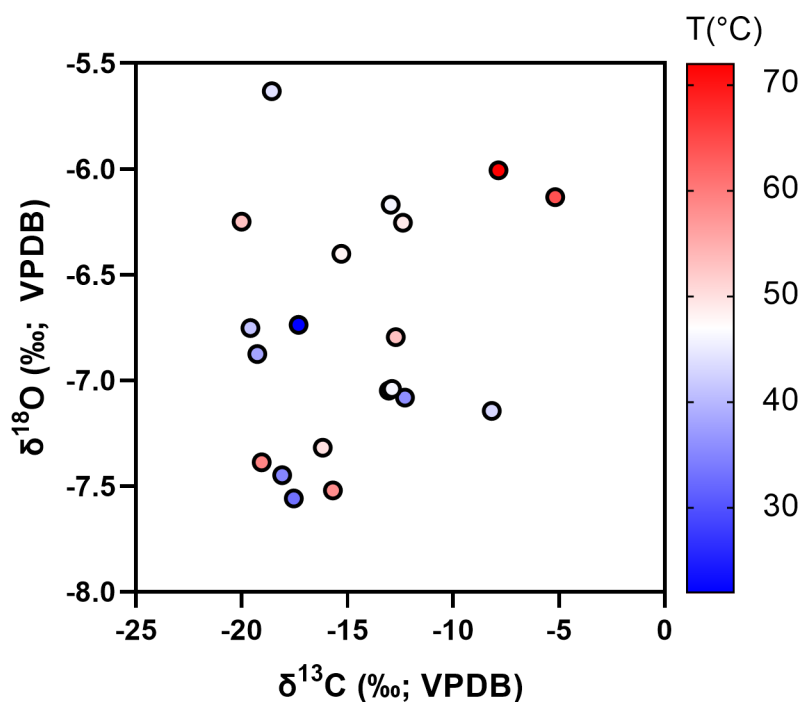***Figure S32.*** Crossplot of calculated T_{47} and $\delta^{13}C$ from calcite spar.

Figure S33. Crossplot of calculated $\delta^{18}O$ and $\delta^{13}C$ from calcite spar, colored by T_{47}.

REFERENCES

Brand, W.A., Assonov, S.S., and Coplen, T.B., 2010, Correction for the 17O interference in δ(13C) measurements when analyzing CO2 with stable isotope mass spectrometry (IUPAC Technical Report): Pure and Applied Chemistry, v. 82, p. 1719–1733, doi:10.1351/PAC-REP-09-01-05.

Chew, D.M., Petrus, J.A., and Kamber, B.S., 2014, U–Pb LA–ICPMS dating using accessory mineral standards with variable common Pb: Chemical Geology, v. 363, p. 185–199, doi:10.1016/j.chemgeo.2013.11.006.

Dennis, K.J., Affek, H.P., Passey, B.H., Schrag, D.P., and Eiler, J.M., 2011, Defining an absolute reference frame for 'clumped' isotope studies of CO2: Geochimica et Cosmochimica Acta, v. 75, p. 7117–7131, doi:10.1016/j.gca.2011.09.025.

Dennis, K.J., and Schrag, D.P., 2010, Clumped isotope thermometry of carbonatites as an indicator of diagenetic alteration: Geochimica et Cosmochimica Acta, v. 74, p. 4110–4122, doi:10.1016/j.gca.2010.04.005.

Ghosh, P., Adkins, J., Affek, H., Balta, B., Guo, W., Schauble, E.A., Schrag, D., and Eiler, J.M., 2006, 13C–18O bonds in carbonate minerals: A new kind of paleothermometer: Geochimica et Cosmochimica Acta, v. 70, p. 1439–1456, doi:10.1016/j.gca.2005.11.014.

Guillong, M., Wotzlaw, J.-F., Looser, N., and Laurent, O., 2020, Evaluating the reliability of U–Pb laser ablation inductively coupled plasma mass spectrometry (LA-ICP-MS) carbonate geochronology: matrix issues and a potential calcite validation reference material: Geochronology, v. 2, p. 155–167, doi:10.5194/gchron-2-155-2020.

Hollocher, K., and Ruiz, J., 1995, Major and Trace Element Determinations on Nist Glass Standard Reference Materials 611, 612, 614 and 1834 by Inductively Coupled Plasma-Mass Spectrometry: Geostandards Newsletter, v. 19, p. 27–34, doi:10.1111/j.1751-908X.1995.tb00149.x.

Huntington, K.W. et al., 2009, Methods and limitations of 'clumped' CO2 isotope (Δ47) analysis by gas-source isotope ratio mass spectrometry: Journal of Mass Spectrometry, v. 44, p. 1318–1329, doi:10.1002/jms.1614.

Kim, S.-T., O'Neil, J.R., Hillaire-Marcel, C., and Mucci, A., 2007, Oxygen isotope fractionation between synthetic aragonite and water: Influence of temperature and Mg2+ concentration: Geochimica et Cosmochimica Acta, v. 71, p. 4704–4715.

Nuriel, P., Wotzlaw, J.-F., Ovtcharova, M., Vaks, A., Stremtan, C., Šala, M., Roberts, N.M.W., and Kylander-Clark, A.R.C., 2021, The use of ASH-15 flowstone as a matrix-matched reference material for laser-ablation U − Pb geochronology of calcite: Geochronology, v. 3, p. 35–47, doi:10.5194/gchron-3-35-2021.

Passey, B.H., Levin, N.E., Cerling, T.E., Brown, F.H., and Eiler, J.M., 2010, High-temperature environments of human evolution in East Africa based on bond ordering in paleosol carbonates: Proceedings of the National Academy of Sciences, v. 107, p. 11245–11249.

Paton, C., Hellstrom, J., Paul, B., Woodhead, J., and Hergt, J., 2011, Iolite: Freeware for the visualisation and processing of mass spectrometric data: Journal of Analytical Atomic Spectrometry, v. 26, p. 2508–2518.

Roberts, N.M.W., Rasbury, E.T., Parrish, R.R., Smith, C.J., Horstwood, M.S.A., and Condon, D.J., 2017, A calcite reference material for LA-ICP-MS U-Pb geochronology: Geochemistry, Geophysics, Geosystems, v. 18, p. 2807–2814, doi:10.1002/2016GC006784.

Taylor, H.P., 1974, The Application of Oxygen and Hydrogen Isotope Studies to Problems of Hydrothermal Alteration and Ore Deposition: Economic Geology, v. 69, p. 843–883, doi:10.2113/gsecongeo.69.6.843.

Vermeesch, P., 2018, IsoplotR: A free and open toolbox for geochronology: Geoscience Frontiers, v. 9, p. 1479–1493, doi:10.1016/j.gsf.2018.04.001.